Oil & Gas Science and Technology – Rev. IFP, Vol. 54 (1999), No. 2, pp. 251-257
Copyright © 1999, Éditions Technip

Multi-Dimensional Modeling of Combustion and Pollutants Formation of New Technology Light Duty Diesel Engines

P. Belardini[1] and C. Bertoli[1]

1 Istituto Motori CNR, Via G. Marconi 6-8, Naples - Italy
e-mails: paola@motori.im.na.cnr.it - bertoli@motori.im.na.cnr.it

Résumé — Modélisation multidimensionnelle de la combustion et de la formation des polluants dans les nouveaux moteurs Diesel automobiles — Dans cet article nous présentons les résultats obtenus en utilisant des outils de simulation de la mécanique des fluides numérique (CFD). À partir de résultats expérimentaux issus de la caractérisation d'un moteur Diesel *common rail*, les constantes empiriques de divers modèles ont été ajustées afin d'obtenir des résultats satisfaisants pour des cas tests représentatifs.

Les principales contraintes des modèles numériques pour obtenir une bonne précision dans les différents cas d'études sont ici analysées. Cette analyse numérique montre que la CFD permet déjà, au stade de développement atteint, d'aider les ingénieurs à définir les stratégies les plus prometteuses pour maîtriser les émissions à l'échappement des moteurs Diesel à injection *common rail*.
Mots-clés : CFD, modélisation, combustion, Diesel, *common rail*.

Abstract — Multi-Dimensional Modeling of Combustion and Pollutants Formation of new Technology Light Duty Diesel Engines *— In the present paper some results, obtained by the use of modern numerical CFD tools, are presented. In particular, starting from the experimental characterization of a common rail DI Diesel engine, the empirical constants of the different submodels were tuned to obtain satisfactory results in some key test conditions.*

The main constraints of numerical models, to obtain a right scaling of pollutants predictions in the different test cases are analyzed. The numerical analysis demonstrates that the numerical CFD tools, at their stage of development, can help the engine designers to define the more promising strategies to obtain tailpipe emission control of common rail Diesel DI engines.
Keywords: CFD, Multi-Dimensional Modeling, Combustion, Diesel, Common Rail.

INTRODUCTION

The direct injection combustion system, due to its advantages in fuel consumption, appears as the key of the successful application of Diesel engines in the passenger cars market. However, the further emission limits reduction planned at the beginning of next century in Europe, will pose some problems to the direct injection Diesel engines (DDI) that, intrinsically, exhibit relatively high NO_x emissions. As matter of fact the NO_x emission limit, reduced up to 0.25 g/km in 2005 regulations (Euro IV stage), appears as a very severe target to reach for this kind of engines.

The mixing process governs the combustion in DI engines. The passenger car engines are obviously geometrically smaller than heavy-duty engines. This leads to reduced free spray length and need of some swirl level during combustion. In order to avoid smoke emission the carbon over oxygen ratio (C/O) must be minimized. This requires enhanced injection pressures (especially in transient conditions) and a reduced discharge area of injection nozzles. These requirements can be matched by the new generation of injection systems based on the common rail technology.

A fully electronically controlled management of injection system opens new ways to controls NO_x emissions like injection pressure regulation speed and load dependent or post-injection ($DeNO_x$ aftertreatment system regulation) [1, 2].

The numerical CFD tools, at their stage of development, can help the engine designers to define the more promising

strategies to obtain tailpipe emission control [3-5]. Their performances cannot be considered predictive in absolute, but tuning the various model constants for a given engine and on a limited number of test cases, the response of different submodels allows the right scaling of the different arrangements of the combustion system.

The present paper some results, obtained by the use of a modern numerical CFD tool, are presented. In particular, starting from the experimental characterization of a common rail engine, the empirical constants of the different submodels were tuned to obtain satisfactory results in some key test conditions. the main problems, related with the various physical sub-models implementation are also discussed.

1 THE MODEL

1.1 The Kiva-3V Modifications

In this work the diesel engine combustion simulations were performed with the Kiva-3V code [6]. To simulate the airflow field, the κ-ε RNG turbulence model in the Han and Reitz [7] form was used. The atomization process was computed using the hybrid model developed by Belardini *et al.* [8] based on both Wave [9] breakup an Tab [10] models. The droplets evaporation model was improved removing the hypothesis of the fuel thermal conductivity assumed as "infinite" and the temperature inside the droplet uniform and equal to its surface temperature value [11]. The development of the ignition model is based on the Hiroyasu method [12] by using the Handerberg et Hase correlation [13]. The NO formation is modeled with Zel'dovich mechanism in the form described by Bowman [14]. Finally the soot formation and oxidation mechanism is coupled with the combustion model by a reduced six steps mechanism in the form developed by Belardini *et al.* [15].

1.2 The Coupled Combustion - NO_x and Soot Model

The soot model here considered was firstly proposed by Leung *et al.* [16] and Fairweather *et al.* [17]. In this model the acetylene is assumed as crucial pyrolytic specie for the nucleation and surface growth processes. Belardini *et al.* [15] implemented a slightly modified version of this model in the standard kinetic routine of Kiva-II code simulating *n*-heptane and tetradecane fuels combustion. In the present paper, a further refinement of the model was obtained adding a coupled mechanism to provide the high temperature combustion not only of the injected fuel but also of the formed acetylene.

The global formulation of the model is a right compromise between a comprehensive description of the in-cylinder soot loading process and the computational cost of full 3D Diesel combustion calculations.

In addition the model used in the present paper, even if simplified, was tested in a variety of conditions by the authors in previous papers giving a sufficient degree of reliability in keeping the experimental findings.

The full coupling with the combustion mechanism and the NO formation model characterizes the soot model in the actual form.

The main model features are the following: the liquid fuel is injected; the fuel vaporization and dispersion are computed as provided by the Kiva-3V code routines. The injected fuel is oxidized at high temperatures by:

$$\text{(R1)}\quad C_nH_m + \left(n + \frac{m}{4}\right)O_2 \overrightarrow{\leftarrow} nCO_2 + \frac{m}{2}H_2O \quad (1)$$

at the rate:

$$\omega_1 = min\,(\omega_{premix1}, \omega_{diff1}) \quad (2)$$

where the premixed and diffusive velocity are:

$$\omega_{premix1} = A_i e^{E_i/T}\left[C_nH_m\right]^c\left[O_2\right]^d \quad (3)$$

$$\omega_{diff1} = C_i\frac{\varepsilon}{\kappa} * min\left(\left[C_nH_m\right], \frac{\left[O_2\right]}{s}\right) \quad (4)$$

Here and in the following the terms in squared parenthesis are molar concentration in mol/cm^3; κ and ε are the turbulent kinetic energy and its dissipation rate; s is the stochiometric ratio. A_i and E_i are respectively the preexponential factor and the activation temperature for the premixed combustion their values are reported later together with the other constants setting; C_i is the proportional factors for the diffusive combustion.

The following three steps describe the Zeldowich mechanism:

$$\text{(R2)}\quad O + N2 \rightleftarrows N + NO \quad (5)$$

$$\text{(R3)}\quad O2 + N \rightleftarrows O + NO \quad (6)$$

$$\text{(R4)}\quad N + OH \rightleftarrows H + NO \quad (7)$$

The Bowman [14] set of rate constants was adopted:

$$\omega_{2f} = 7.6*10^{13}\ \exp\left[-38\,000/T\right] \quad (8)$$

$$\omega_{2b} = 1.6*10^{13} \quad (9)$$

$$\omega_{3f} = 6.4*10^{9}T*\exp\left[-3150/T\right] \quad (10)$$

$$\omega_{3b} = 1.5*10^{9}T*\exp\left[-19\,500/T\right] \quad (11)$$

$$\omega_{4f} = 4.1*10^{13} \quad (12)$$

$$\omega_{4b} = 2.0*10^{14}\ \exp\left[-23\,650/T\right] \quad (13)$$

Simultaneously the fuel vapor undergoes to acetylene by a single step reaction:

$$\text{(R5)} \qquad C_nH_m \rightarrow \frac{n}{2}C_2H_2 + \frac{m}{2}H_2 \tag{14}$$

whose reaction rate is:

$$\omega_5 = A_5 e^{-E_5/T} \left[C_n H_m\right] \tag{15}$$

A three-step soot formation and oxidation model performs the soot loading computations for each computational cell using the mechanism:

$$\text{(R6)} \quad C_2H_2 \rightarrow 2C + H_2 \text{ nucleation} \tag{16}$$

$$\text{(R7)} \quad C_2H_2 + nC \rightarrow (n+2)C + H_2 \text{ surface growth} \tag{17}$$

$$\text{(R8)} \quad C + 0.5O_2 \rightarrow CO \text{ carbon oxidation} \tag{18}$$

The corresponding reaction rates are the followings:

$$\omega_6 = A_6 e^{-E_6/T} \left[C_2H_2\right] \tag{19}$$

$$\omega_7 = A_7 e^{-E_7/T} (\rho N)^{1/6} [C]^{1/3} \left[C_2H_2\right] \tag{20}$$

$$\omega_8 = A_8 e^{-E_8/T} T^{1/2} (\rho N)^{1/3} [C]^{2/3} \left[O_2\right] \tag{21}$$

Here:

ρN is the number density [particles/cm^3];

T is the cell temperature [K];

MW_c is the carbon molecular weight;

$\rho_c = 1.8$[g/cm^3] is the soot density;

K is the Boltzmann constant.

Also the formed acetylene is oxidized at high temperature by a single step stochiometric reaction:

$$\text{(R9)} \qquad C_2H_2 + \frac{5}{2}O_2 \Leftrightarrow 2CO_2 + H_2O \tag{22}$$

Characterized by the rate: $\rightleftarrows$

$$\omega_9 = min(\omega_{premix\,9}, \omega_{diff\,9}) \tag{23}$$

where the premixed and diffusive velocity are:

$$\omega_{premix9} = A_9 e^{E_9/T} \left[C_2H_2\right]^a \left[O_2\right]^b \tag{24}$$

$$\omega_{diff\,9} = C_9 \frac{\varepsilon}{\kappa} * min\left(\left[C_2H_2\right], \frac{\left[O_2\right]}{s}\right) \tag{25}$$

To take into account the agglomeration phenomenon the following step is added to the mechanism:

$$\text{(R10)} \qquad nC \rightarrow C_n \text{ agglomeration} \tag{26}$$

at the rate:

$$\omega_{10} = A_{10} T^{1/2} (\rho N)^{11/6} [C]^{1/6} \tag{27}$$

where:

$$A_{10} = 2 * 9 * \left(6 * MW_c / \pi \rho_c\right)^{1/6} \sqrt{6K/\rho_c} \tag{28}$$

The combustion model includes a simplified ignition delay computation method. The high temperature fuel and acetylene oxidation start in each computational cell when it reaches the condition:

$$\int_0^{t_{ig}} \frac{1}{\tau_d} d\tau = 1 \tag{29}$$

For the ignition delay time td the correlation by Hardenberg and Hase [13] was used:

$$\tau_d = \frac{n}{6}\left(0.36 + 0.22 S_p\right) * \exp\left(E_A\left(\frac{1}{RT} - \frac{1}{17190}\right) + \left(\frac{21.2}{p - 12.4}\right)^{0.63}\right) \tag{30}$$

where:

0 is the time at which injection starts;

n is the engine speed rpm (tr/min);

T is the cell temperature (K);

p is the cell pressure (bar);

S_p is the mean piston speed (m/s).

This ignition delay mechanism is sensitive to the fuel cetane number via the energy activation term:

$$E_A = \frac{618\,840}{CN + ef} [J/mol] \tag{31}$$

With ef empirical factor that needs a tuning, in order to obtain a better fitting of the experimental data in a number of test cases [18].

The constants of the kinetic mechanism are:

$A_1 = 0.64 * 10^{11}$	$E_1 = 16\,300$
$A_5 = 2.4 * 10^{11}$	$E_5 = 25\,000$
$A_6 = 0.95 * 10^{8}$	$E_6 = 21\,100$
$A_7 = 0.24 * 10^{8}$	$E_7 = 13\,100$
$A_8 = 1.6 * 10^{3}$	$E_8 = 23\,800$
$A_9 = 8.5 * 10^{9}$	$E_9 = 16\,300$

A significant modification to the code consisted in the adoption of a different scheme to solve the stiff system deriving from the kinetic reaction mechanism adopted in combustion computations. As matter of the fact in the original version of the Kiva-3V code the set of the kinetic chemical reaction is sequentially solved equation after equation. Considering that the reaction rates values may be

strongly different one each other, a mechanism is provided to prevent that at the computational time step some specie may be driven negative. Therefore the choice of sequence used to solve the set of equation has influence on the computed updated values of the specie densities, that are different in dependence of the sequence adopted.

As consequence a modification was introduced aimed to solve simultaneously the set of the kinetic equations: the method used was based on the Burlisch-Stoer algorithm, using a semi-implicit extrapolation procedure to discretize the differential equations in the time sub-steps [18].

Finally the six-equilibrium reaction scheme, present in the standard version of the code, was retained in the present set of calculations. This scheme includes the water-gas equilibrium.

2 THE ENGINE AND TEST CASES

For this study a common rail FIE equipped DDI engine (Table 1) was chosen.

TABLE 1

Engine characteristics

Engine	Fiat M 714 (1910 JTD)
Bore (mm)	82
Stroke (mm)	90.4
Compression ratio	18/1
Total displ. (cm^3)	1910
Rated power (kW)	77 at 4000 tr/min
Rated torque (Nm)	255 Nm at 2000 tr/min
Injection system	Common rail
Turbocharged after-cooled	Garret GT15 with w.g.
EGR	Electronically controlled

The engine was equipped with a piezo-quartz transducer to detect the indicated pressure and with a resistive transducer to detect the injection pressure at the electroinjector fuel inlet (after the rail). One of the injectors type was instrumented with a Microepsilon needle lift transducer.

A shaft encoder with a maximum angular resolution of 0.1 crank angle degree allows the synchronization of the various signals. A Bosch development system allowed to read and write interactively the ECU to set the engine test points.

Five engine points, at low speed and low load, were assumed as representative of the engine behavior in the urban driving schedule of the European test procedure for exhaust emission ranking. In particular 2 bar BMEP and 2000 tr/min varying rail pressure, engine timing, EGR and pilot injection were chosen (Table 2).

As concerns the exhaust pollutant measurements, the gaseous emissions were measured on raw exhausts. To improve the reliability of the particulate measurements and its characterization both the raw exhaust sampling method and the diluted one were adopted. Preliminary comparative tests between the two sampling methods confirmed that the results in terms of total particulate, as well as of insoluble (IOF) and dicloromethane soluble (SOF) fraction measurements, were consistent.

TABLE 2

Engine test cases for comparisons with computations

Test	# 1	# 2	# 3	# 4	# 5
tr/min	2000	2000	2000	2000	2000
Mass/cyc.	8.7 mg	8.7 mg	8.7 mg	8.7 mg	8.7 mg
Rail press.	350 bar	550 bar	800 bar	520 bar	520 bar
Start ET main (c.a.)	–10 BTDC	–8 BTDC	–7 BTDC	–2.5 BTDC	–2.5 BTDC
Start ET Pilot	–	–	–	–27 BTDC	–
EGR (%)	0	0	0	30	30

3 RESULTS

3.1 Combustion Evolution

The computational runs were performed, during compression stroke starting from the inlet valve closure BTDC. The inlet pressure, temperature and species mass fractions of the different numerical test cases were computed by simple thermodynamic calculations. A swirl ratio value of 3.5, measured by steady state impulse wheel anemometer, was assumed as representative of the mean flow conditions at the beginning of compression stroke. To compute the initial turbulent kinetic energy (TKEI) the Abraham and Bracco correlation was used. However it can be noted that, also varying this value of ± 50%, the predictions of TKE at the end of the compression stroke are quite the same. So the uncertainty in choosing this value is practically insignificant for the spray and combustion computations. In Figures 1 and 2 the computed indicated pressure is compared with the numerical one for the selected test cases.

The accuracy of calculation seems satisfactory. It can be noticed that the computations under estimate the measured pressure during the expansion stroke. This effect, typical of Kiva-3V combustion computations, may be ascribed both over estimation of heat loss on the wall as well as to a too simplified description of the combustion of the mass of fuel burning near the chamber wall.

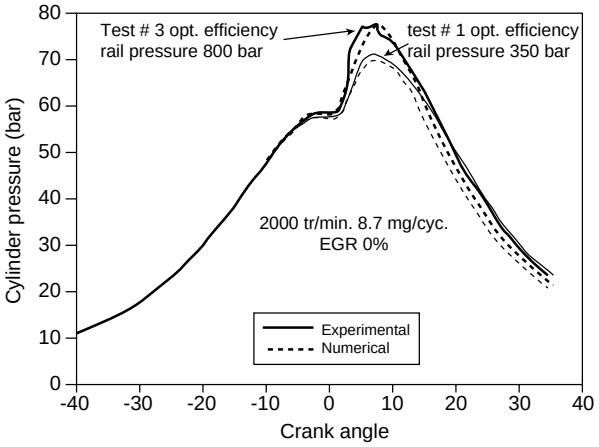

Figure 1

Comparison between computed and measured indicated pressure: test # 1, # 3: 2000 tr/min, rail pressure 350-800 bar, and 8.7-mg/cyc. inj. mass without EGR engine setting for min. fuel consumption.

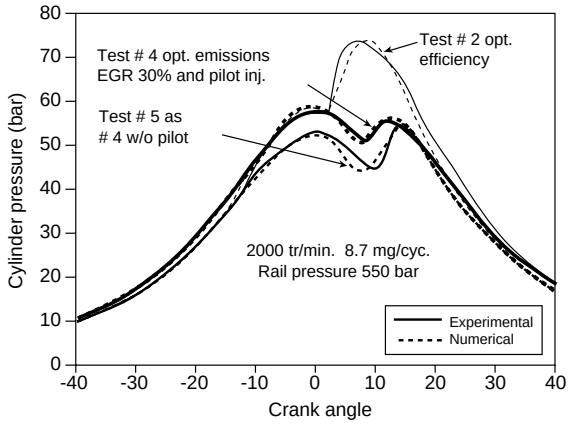

Figure 2

Comparison between computed and measured indicated pressure: test # 2, # 4 and # 5. 2000 tr/min, 8.7 mg/cyc. inj. mass, rail pressure 550 bar; test # 2 w/o EGR engine setting for min. fuel consumption; test # 4 EGR 30% and pilot injection, engine setting for low NO_x emission; test # 5 as test # 4 but w/o pilot injection.

All numerical calculations were performed with the same tuning of the various model constants with the exception of the test case # 4.

When the engine operates with pilot injection, appears very difficult obtain satisfactory results the same setting of model constants adopted in adopted in other test cases. In particular it was necessary to significantly change both the constant *ef* in Equation (31) and the proportional factor C_1 for the diffusive combustion in Equation (4).

This result is no surprising looking at the shape of the rate of heat release when the pilot injection is active (Fig. 3).

The adoption of a dwell angle between the pilot and the main injection > 10° c.a. (in our case > 20 c.a.) produces two separate heat release during combustion cycle. So the main effect of the pilot injection, from the point of view of the combustion evolution, is the production in the combustion chamber of a sort of internal EGR located near the incoming fuel jets. During the separation angle between pilot and main injection the swirl distributes the combustion products in the combustion chamber. Clearly the ignition delay time correlation works, in the case of pilot injection, out of the range of pressures and temperatures in witch was previously tested so a retuning is needed.

More difficult to explain the need of changing the setting of the proportional factor C_1 for the diffusive combustion.

Because of the physical delays in actuating the electro-hydraulic system that controls the injector needle opening, about 250 μs are needed (3 c.a. at 2 000 tr/min) to open and close the needle. So the initial injection velocity cannot be easily computed by using the hydraulic flow relations because of the partial opening of the needle. This uncertainty probably produces a strong inaccuracy on modeling of spray dispersion deriving from pilot injection and this effect leads a different setting of the most controlling constant of the combustion model. It must be noticed that, in absence of experimental data, it was assumed an initial velocity of the pilot injection of 60 m/s and a pilot mass of 1mg in all test conditions.

The previously stated problem is a serious limitation of the model predictivity. However, the adoption of two different set of constants for pilot and main injection during the same run, an acceptable behavior of the computed heat release shape can be obtained (Fig. 3, dotted line). A number of the run performed varying the dwell angle and the main injected mass demonstrated the effectiveness of the approach adopted.

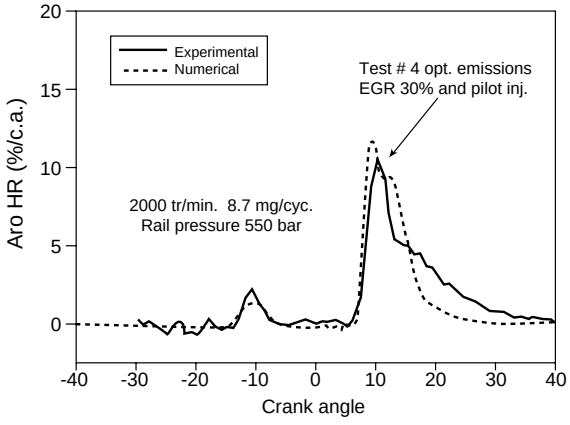

Figure 3

Computed and measured apparent rate of heat release: test # 4 with pilot injection.

3.2 Pollutants Predictions

For the reasons discussed in the previous section the computations underestimate the measured exhaust NO_x concentration. The fit with the exhaust was obtained by multiplying the computed NO_x by a factor $\beta = 6.5$.

It must be noted that the numerical NO_x data as well as the experimental ones are reduced to the molecular weight of NO_2 as prescribed by the all exhaust emissions regulations in Europe and United States. As concerns exhaust soot emission predictions, numerical results were directly compared with the experiments without any further retuning.

In Table 3 the computed results are reported in comparison with experiments.

TABLE 3

Computed and measured exhaust emissions

T	NO_x Com. ppm	NO_x Meas. ppm	Δ (%)	Soot com. g/kg	Soot meas. g/kg	Δ (%)
# 1	350	360	-2.8	0.42	0.50	-16
# 2	440	440	-	0.21	0.22	-4.5
# 3	530	550	-3.6	0.10	0.11	-9.1
# 4	150	170	-11.8	1.0	0.87	14.9
# 5	165	180	-8.3	0.40	0.36	11.1

Even if the results, in terms of computed exhaust soot mass prediction, differ significantly from measurements, nevertheless is noticeable that the trends are fully reproduced by computations.

In the Figure 4, as example, the computed soot loading versus crank angle, for test # 2, # 4 and # 5, is reported. The tests are all referred to a rail pressure of 550 bar:

– in test # 2 (optimum fuel consumption setting) the engine operates without EGR and injection timing able to produce the start of combustion near TDC;
– in test # 4 (engine optimized for low NO_x and noise emissions) the pilot injection is active as well as the EGR at a rate of 30% measured by CO_2 method;
– in test # 5, performed in the same conditions of test # 4, the pilot injection was inhibited.

The diagram gives a clear explanation of some peculiarities of common rail engines. Firstly even if it's a well known that the EGR and retarding timing practice has detrimental effects on soot emission, the very low soot emission of obtained using common rail injection systems allows to operate in these conditions without strong penalties in soot emissions. On the other hand the pilot injection adoption (mandatory needed to reduce the combustion noise) produces a remarkable increase of final soot emission. This effect can be ascribed to the initial soot formation phase, during the pilot injection that cannot be oxidized and so contributes to the rise of the final soot emission.

As concerns NO_x emissions, within the limits of the model previously discussed, also the computations demonstrate that the effect of pilot injection doesn't influence this emission.

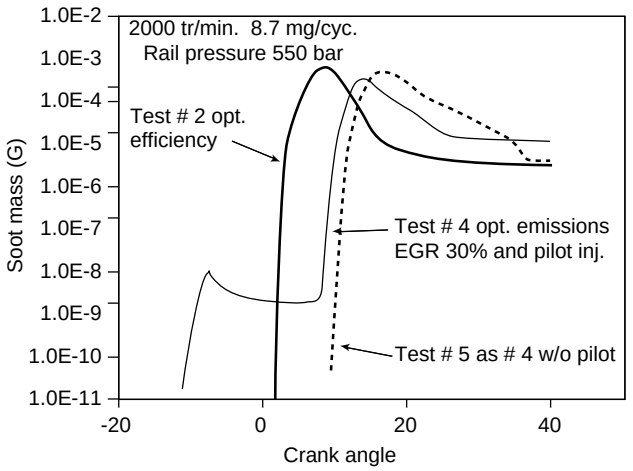

Figure 4

Soot loading in test cases # 2, # 4, # 5.

CONCLUSION

The combustion behavior of a light duty Diesel DI engine, equipped with common rail injection system, was investigated by using an improved version of the Kiva-3V CFD code. The study was limited to a specific point of the engine map, actually 2000 tr/min and about 2 bar BMEP. In this point some setting of engine were changed including rail pressure, injection timing, EGR and pilot injection. The comparison with experimental results demonstrates the effectiveness of the code to well reproduce the experimental trends. However the results cannot be considered fully satisfactory. As matter of the fact the lack of predictivity of NO_x emission and combustion evolution during the expansion stroke it was quite evident. In addition in the case of pilot injection adoption, it was impossible to obtain satisfactory results with the same setting of the combustion model adopted to describe the main injection process. New experimental detailed data on injection and combustion process during the pilot injection will allow a new formulation of spray model and the implementation of a new low temperature chemistry able to solve these problems.

REFERENCES

1 Stummp, G. and Ricco, M. (1996) Common Rail-An Attractive Fuel Injection System for Passenger Car DI Diesel Engines. *SAE Paper*, 960870.

2 Guerrassi, N. and Dupraz, P. (1998) A Common Rail System for High Speed Direct Injection Diesel Engines. *SAE Paper*, 9808803.

3 Beatrice, C., Belardini, P, Bertoli, C., Cameretti, M.C. and Del Giacomo, N. (1996) An Assessement of Predictivity of CFD Computations of Combustion and Pollutants Formation in DI Diesel Engines. *SAE Paper*, 962055.

4 Patterson, M.H., Kong, S.C., Hampson, J.H. and Reitz R.D. (1994) Modelling the Effects of Fuel Injection Characteristics on Diesel Engine Soot and No_x Emissions. *SAE Paper*, 940523.

5 Rutland, C.J. *et al*. (1995) Progress Towards Diesel Combustion Modelling. *SAE Paper*, 952429.

6 Amsden, A.A. (1997) Kiva-3V: A Block structured Kiva Program for Engines with Vertical or Canted Valves, *LA-13313-MS*, Los Alamos.

7 Han, Z. and Reitz, R.D. (1995) Turbulence Modelling of Internal Combustion Engines using RNG k-ε Models. *Comb. Sci. Tech.*, **106**, 267.

8 Beatrice, C., Belardini, P., Bertoli, C. and Cameretti, M.C. (1995) Fuel Jet Models for Multi-Dimensional Diesel Combustion Calculation: an Update. *SAE Paper*, 950086.

9 Reitz, R.D. (1987) Modelling Atomisation Processes in High-Pressure Vaporising Sprays. *Atomisation and Sprays Tech.*, **3**, 309-337.

10 O'Rourke, P.J. and Amsden, A.A (1987) The Tab Method for Numerical Calculation of Spray Droplet Break-up. *SAE Paper*, 872089.

11 Bertoli, C. and Migliaccio, M. (1998) A Finite Conductivity Model for Diesel Spray Evaporation. *ILASS- Europe'98*.

12 Nishida, K. and Hiroyasu, H. (1989) Simplified Three-Dimensional Modelling of Mixture Formation and Combustion in a DI Diesel Engine. *SAE Paper*, 890269.

13 Hardenberg, H.O. and Hase, F.W. (1979) An Empirical Formula for Computing Pressure Rise Delay of a Fuel from its Cetane Number and from Relevant Parameters of DI Diesel Engines. *SAE Paper*, 790493.

14 Bowman, C.T. (1975) Kinetics of Pollutant Formation and Descruction in Combustion. *Prog. Energy Combust. Sci.*, **1**, 33-45.

15 Belardini, P., Bertoli, C., Beatrice, C., D'Anna, A. and Del Giacomo, N. (1996) Application of a Reduced Kinetic Model for Soot Formation and Burnout in Three-Dimensional Diesel Combustion Computations. *26th International Symposium on Combustion*, The Combustion Institute, 2517-2524.

16 Leung, K.M., Lindsedt, R.P. and Jones, W.P. (1991) A Simplified Reaction Mechanism for Soot Formation in Non-Premixed Flames. *Combustion and Flames*, **87**, 289-305.

17 Fairweather, M., Jones, W.P., Ledin, H.S. and Lindstedt, R.P. (1992) Prediction and Soot Formation in Turbulent Non-Premixed Propane Flames. *24th Symposium (International) on Combustion*, The Combustion Institute, 1067-1074.

18 Stoer, J. and Burlish, R. (1980) *Introduction to Numerical Analysis*, Springer-Verlag, New York.

Final manuscript received in March 1999